An Autonomous Thermal Scanning System with Which to Obtain 3D Thermal Models of Buildings

58

Antonio Adán, Samuel A. Prieto, Blanca Quintana, Tomás Prado, and Juan García

Abstract

This paper presents a mobile platform that autonomously collects 3D thermal/coloured data and obtains a raw 3D thermal model of the insides of buildings. This platform has been developed with two objectives, the first of which is to develop a new hybrid 3D colour/thermal laser scanner system that will provide 3D thermal points of the 360 × 180 space. The second consists of making the earlier thermal scanner autonomous, such that the best scanner positions required to completely cover the scene can be carried out. This entails proposing an original and efficient new next-best-thermal-scan algorithm (NBTS). After collecting, aligning and mixing 3D thermal data from different positions of the scene, a complete thermal point cloud of the scene is generated. The output of the autonomous system is a raw 3D thermal model of a scene, which can be further processed. The system has been tested in the insides of buildings under occlusion conditions, providing promising results.

Keywords

3D laser scanner • Thermal camera • 3D thermal modelling

58.1 Introduction: A Brief State of the Art

The monitoring and inspection of the energy efficiency of buildings have taken place for many years and have, to date, primarily been carried out by humans carrying thermal cameras. This signifies that 2D thermal imaging and, more precisely, indoor thermography, has been used to visually detect thermal characteristics, such as thermal bridges, a loss of energy or humidity. The world of the automatic 3D thermal modelling of buildings is, however, now flourishing with the advent of the latest precise 3D sensors, reliable mobile robots and efficient AI algorithms [1].

The autonomous thermal scanning problem appeared as a new and challenging subject in the last decade. However, little research has been carried out to date, and only partial aspects of the whole problem have been solved. The vast majority of the existing methods are focused on the thermal sensorial system, which is essentially composed of LiDARs [2], photogrammetric cameras [3] or depth cameras [4], all of which are combined with thermal cameras through the use of different

A. Adán (✉) · S. A. Prieto · B. Quintana · T. Prado · J. García
Castilla La Mancha University, Ciudad Real, Spain
e-mail: Antonio.Adan@uclm.es

S. A. Prieto
e-mail: Samuel.Prieto@uclm.es

B. Quintana
e-mail: Blanca.Quintana@uclm.es

T. Prado
e-mail: Tomas.Prado@uclm.es

J. García
e-mail: Juan.GAguilar@uclm.es

I. Mutis and T. Hartmann (eds.), *Advances in Informatics and Computing in Civil and Construction Engineering*,
https://doi.org/10.1007/978-3-030-00220-6_58

methodologies. However, these systems collect only 3D thermal data of the part of the scene that is covered by the field of view of the thermal camera. Additionally, autonomy is frequently tackled not by a robot, but by a human being carrying or pushing the whole sensorial system [5]. Other indoor thermal mapping approaches are commanded or teleoperated, as is the case of that presented by Mader et al. [6]. This is a complex system composed of three UAVs equipped with a thermal camera and laser scanner, which is used for building inspection tasks.

Very few autonomous platforms have been developed to date. A representative example of an autonomous system is that of Borrmann et al. [7]. This is a thermal scanning mobile system that automatically creates low resolution thermal mesh models of the indoors of buildings. The robot initially uses a 2D next best view approach until it is assumed to be inside a room. From one position of the robot, the system covers 360-thermal scans but with a limited vertical FOV. Since the platform cannot rotate vertically, the completeness of the thermal model of the scene is not guaranteed.

In this reduced world of autonomous mobile thermal scanning systems, our principal contributions are as follows.

First, our scanning platform is complete in the sense that the sensorial setup (3D laser scanner + colour camera + thermal camera) can obtain 360 thermal data per scan and, if necessary, rotate vertically in order to cover a higher vertical FOV of the scene. Second, our original 3D next best view algorithm is based on maximising the visibility of the structural components of the building (i.e. ceiling/ground/walls) from the next robot position and is able to work in the presence of occlusion. Third, an original robot positioning and navigation procedure is proposed.

58.2 An Overview of the Autonomous Thermal Scanner System

A brief summary of our system is provided as follows. The scanning platform is prepared to obtain separate 3D thermal models of each room on the floor of a building, which are subsequently aligned to eventually generate a single model. Since we are dealing with inhabited environments, a room should probably be sensed from different robot positions, which are calculated by our NBTS algorithm. This is a probabilistic-based approach that minimises the uncertainty of finding new regions of structural elements (i.e. walls, floor and ceiling) (SEs) in the next scan position. In each new scan, the already visible (sensed) space is discretized into minute voxels and those that lie on the voxels of the recognised SEs are characterised by their colour and temperature. When no new SE voxels are found, a stopping criterion is satisfied, and the final 3D thermal model of the room is created. The robot then moves towards the door of the room, enters an adjoining room and runs a new room-scanning process.

Figure 58.1a shows a flowchart in which the scanner and the actions of the robot appear separately but are, simultaneously, connected at several points. The scanner is focused on taking 360-thermal scans, generating the obstacle map and calculating the position of the next best thermal scan. With regard to the robot, it provides the odometry data, aligns the

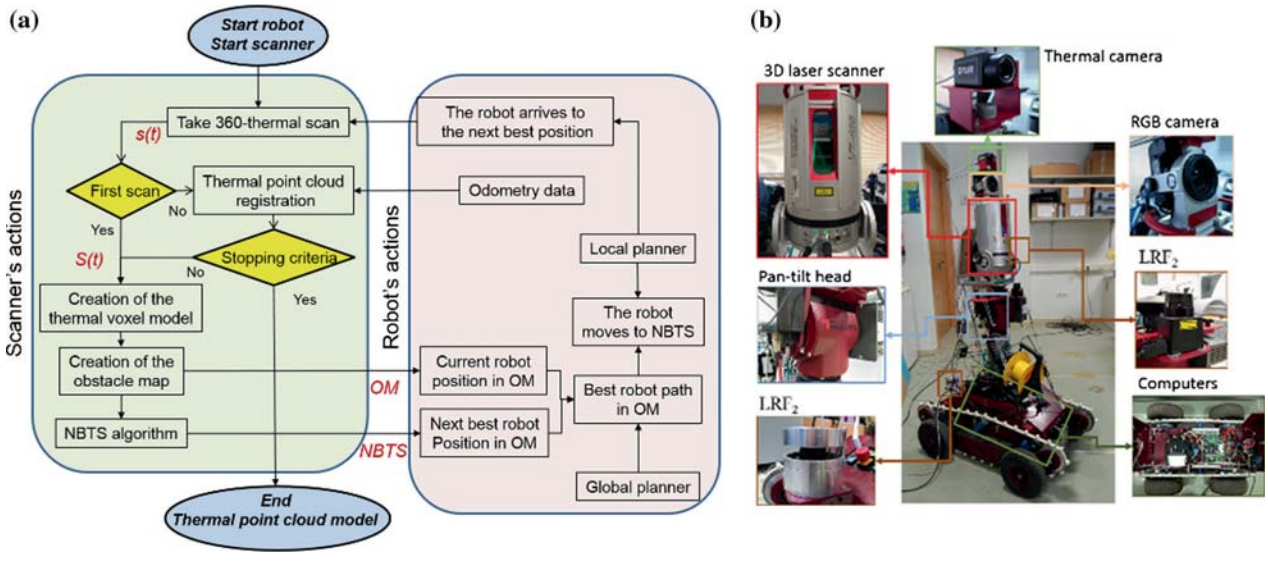

Fig. 58.1 **a** Performance of the autonomous thermal scanner system. **b** Components of MoPATD

accumulated thermal data with the current thermal point cloud and navigates safely towards the next position calculated by using its global and local planners. A description of the components of the mobile platform follows.

We have implemented the autonomous scanning system on the MoPATD (Mobile Platform for Autonomous Thermal Digitization) platform, which is composed of several components: a Robotnik Guardian mobile robot, a Riegl VZ-400 3D laser scanner, an RGB Nikon D90, a FLIR A65 thermal camera and two Hokuyo URG-04LX-UG01 laser range finders (denominated as LRF1 and LRF2). The whole system is managed by two computers. Figure 58.1b shows the components of MoPATD.

The mobile robot is 103.87 cm (length) × 78.20 cm (width) × 100 cm (height) in size and weighs 111.22 kg. Two 300 W motors are used to power four wheels. The speed of the mobile platform is 20 cm/s at maximum velocity. LRF1, like LRF2, has a maximum range of 5.60 m, a scan angle of 240° and a data rate of 10 Hz.

The 3D scanner is used to collect 3D dense point clouds in a range of 500 m. A single scan covers an area of 360° × 100°, takes around 73 s and yields 8.5 million coordinates in the scanner reference system. In our experimental tests, the horizontal and vertical angular resolution was set to 0.065°. The accuracy of the distances measured is 5 mm and the precision is 3 mm (one sigma 100 m range). The scanner is placed on a pan-tilt servo motor, signifying that it can be rotated vertically.

The RGB Nikon D90 camera has a field of view (FOV) of 94° × 70° and provides images of 4288 × 2848 pixels. The FLIR A65 thermal camera has a resolution of 640 × 512 pixels, with a FOV of 45° × 37° at a frequency of 30 Hz. The temperature range in the High Mode is between 233° and 823° K with a precision of 0.4° K.

58.3 Obtaining a 360-Thermal Point Cloud

58.3.1 Obtaining a Single 3D Thermal Shot

Before obtaining 3D thermal data, several off-line processes concerning vignetting, intrinsic and extrinsic calibrations are tackled. The intrinsic calibrations of both the RGB and thermal cameras have been carried out following the standard method of [8]. The vignetting effect have been empirically corrected after calculating a function that provides the radial temperature loss.

The external calibration consists of finding the projective transformation M between the laser scanner and the thermal camera coordinate systems. Assuming that (X_p, Y_p, Z_p) are the coordinates of a certain point in the scanner coordinate system and that (X_f, Y_f) are the coordinates (in pixels) of the corresponding point projected onto the thermal image, matrix M is represented as a 3 × 4 matrix in Eq. (58.1).

$$\begin{pmatrix} \lambda X_f \\ \lambda Y_f \\ \lambda \end{pmatrix} = \begin{pmatrix} r_{11} & r_{12} & r_{13} & r_{14} \\ r_{21} & r_{22} & r_{23} & r_{24} \\ r_{31} & r_{32} & r_{33} & r_{34} \end{pmatrix} \begin{pmatrix} X_p \\ Y_p \\ Z_p \\ 1 \end{pmatrix} \tag{58.1}$$

In order to automatically recognize a point in the 3D space and its projected pixel in the thermal image, we have designed targets with discriminative properties as regards reflectance and temperature. The target consists of a small plastic ice cube to which a reflective circle is attached. Owing to its high reflectivity and low temperature the target is easily identified in the reflectance polar image and thermal image, respectively (see Fig. 58.2a).

If $r_{34} = 1$ and λ is removed, Eq. (58.1) is extended to n points in Eq. (58.2), which is resolved for variables $r_{11}, r_{12}, \ldots, r_{33}$.

$$\begin{pmatrix} X_{f1} \\ Y_{f1} \\ \vdots \\ X_{fn} \\ Y_{fn} \end{pmatrix} = \begin{pmatrix} X_{p1} & Y_{p1} & Z_{p1} & 1 & 0 & 0 & 0 & 0 & -X_{f1}X_{p1} & -X_{f1}Y_{p1} & -X_{f1}Z_{p1} \\ 0 & 0 & 0 & 0 & X_{p1} & Y_{p1} & Z_{p1} & 1 & -Y_{f1}X_{p1} & -Y_{f1}Y_{p1} & -Y_{f1}Z_{p1} \\ \vdots & \vdots & \vdots & \vdots & \vdots & \vdots & \vdots & \vdots & \vdots & \vdots & \vdots \\ X_{pn} & Y_{pn} & Z_{pn} & 1 & 0 & 0 & 0 & 0 & -X_{fn}X_{pn} & -X_{fn}Y_{pn} & -X_{fn}Z_{pn} \\ 0 & 0 & 0 & 0 & X_{pn} & Y_{pn} & Z_{pn} & 1 & -Y_{fn}X_{pn} & -Y_{fn}Y_{pn} & -Y_{fn}Z_{pn} \end{pmatrix} \begin{pmatrix} r_{11} \\ r_{12} \\ r_{13} \\ r_{14} \\ r_{21} \\ r_{22} \\ r_{23} \\ r_{24} \\ r_{31} \\ r_{32} \\ r_{33} \end{pmatrix} \tag{58.2}$$

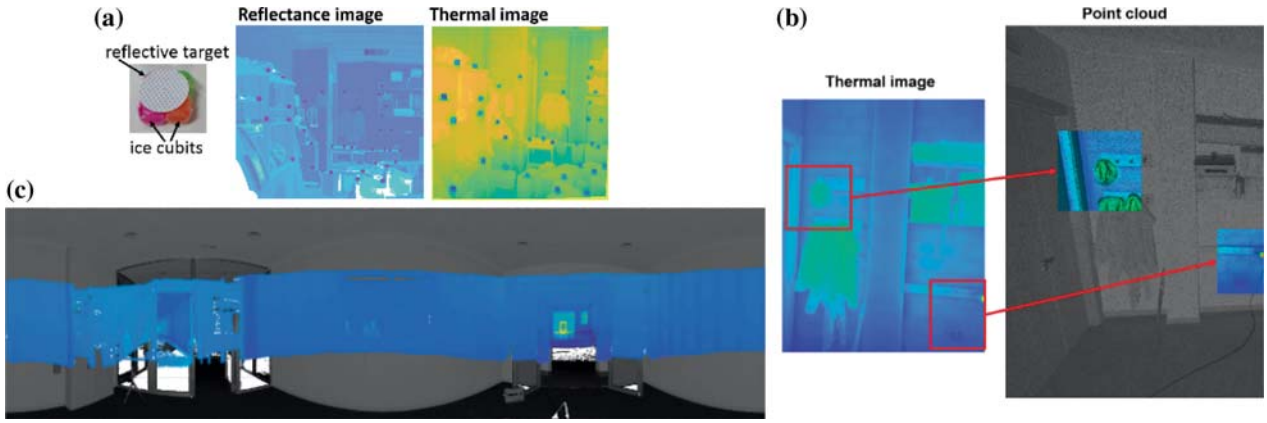

Fig. 58.2 **a** Reflectance and thermal images with reflective frozen targets used for calibration. Targets are clearly identified in both images. **b** A detail of a single thermal image and the corresponding 3D points. **c** A 360-thermal point cloud represented on a polar image

In a matrix notation, the corresponding equation $\boldsymbol{C} = \boldsymbol{WP}$ is solved in Eq. (58.3) and the matrix M is eventually found.

$$\boldsymbol{P} = \left(\boldsymbol{W}^{\boldsymbol{T}}\boldsymbol{W}\right)^{-1}\boldsymbol{W}^{\boldsymbol{T}}\boldsymbol{C} \tag{58.3}$$

58.3.2 360-Thermal Point Cloud from a Position of the Robot

After calculating matrix M, the temperature is assigned to each 3D point in five sequential steps, thus obtaining a thermal point cloud of the scene.

The pant-tilt head is fixed at a certain tilt angle α. Initially, $\alpha = 0$, and the set scanner-RGB camera-thermal camera remains in a vertical position.

The laser scanner takes a 360-scan and captures n points, with coordinates $\left(X_{p(i)}, Y_{p(i)}, Z_{p(i)}\right), i = 1, 2, \ldots, n$, according to a specific vertical FOV of the scanner.

1. The thermal (and the RGB) camera rotates around the Z-axis of the scanner taking m shots, thus covering a horizontal range of 360°. Note that the scanner, the RGB and the thermal camera rotate together.
2. The coordinates $\left(X_f, Y_f\right)_k$ in the k-th thermal shot corresponding to a subset of points $\left(X_p, Y_p, Z_p\right)_k$ are then calculated taking into account the k-th horizontal rotation angle of the camera. Finally, the temperature is assigned to the points $\left(X_p, Y_p, Z_p\right)_k$. Figure 58.2b shows an example of this.
3. If $\alpha \neq 0$, the thermal point cloud is aligned with the initial scanner coordinate system and the accumulated 360-thermal point cloud is stored (Fig. 58.2c).

58.4 Autonomous Thermal Scanning

58.4.1 3D Data Processing to Find the Next Thermal Scan

Since the objective is to produce a 3D thermal model of the indoor of a building, our scanning method is focused on collecting as much temperature data regarding the structural components as possible. The majority of the current 3D mapping approaches (not exclusively thermal mapping) that aim to create a 3D model of a building may be inefficient because the scanning stage is viewed as a process in which the objective is to accumulate data, no matter what the origin of the data is [9]. However, our NBTS algorithm is based on collecting the thermal data of the hypothetical potential structural elements in the scene.

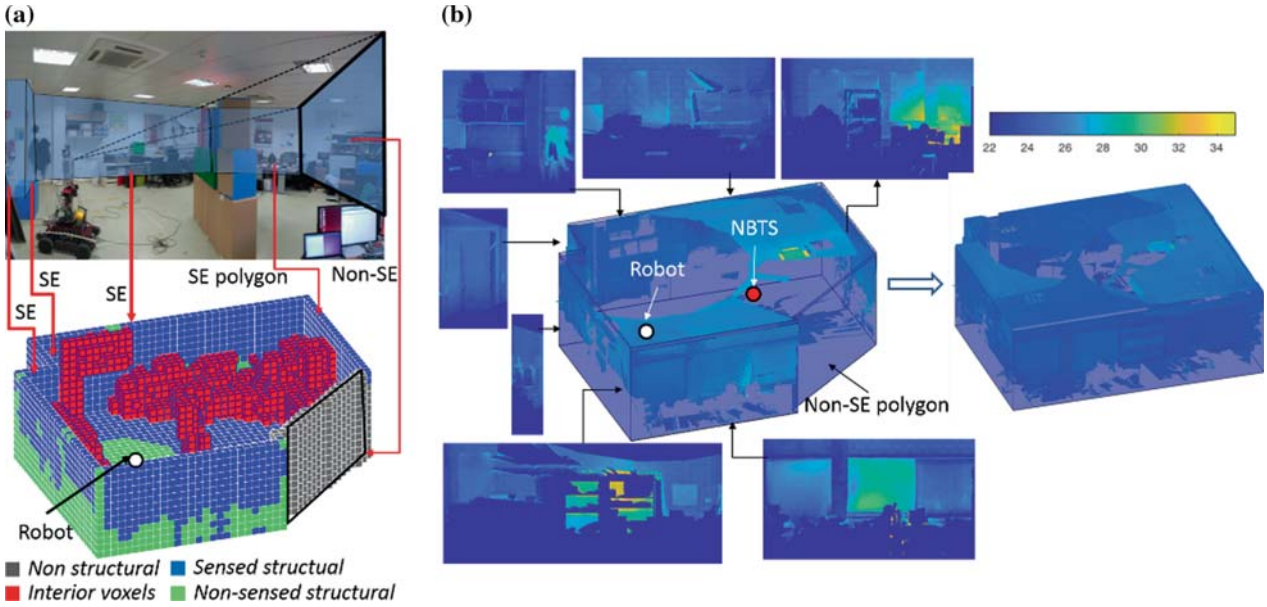

Fig. 58.3 **a** Example of a voxel space for the first thermal scan with SE and Non-SE polygons. **b** RoI of the scene with the associated temperature, the NBTS (first candidate in list $\{l\}_{NBTS}$) and the thermal orthoimages of the walls detected in the RoI (left). Thermal model after three thermal scans (right)

After the t-th scan, we define a temporal region of interest (RoI) of the scene as the polyhedron that contains the accumulated thermal point cloud. In contrast with other scanning methods [10], the boundaries (i.e. the RoI) of our workspace are not hypothesized, but rather update as a new scan is taken. This makes our approach versatile for arbitrarily-shaped scenes.

In order to work in a structured dataset, the 3D space inside the RoI-which includes the 3D sensed points and their associated temperatures—is discretised into voxels, each containing the average temperature of the points inside the voxel. If a voxel does not contain data, no temperature is associated with it. We thus generate a voxel space in which the RoI is made of polygons labelled as *structural element* (SE) and *non-structural element*. This classification is carried out by following the SVM learning algorithm published in [11]. Intuitively, an SE polygon contains one or more zones of concentrated sensed voxels, whereas a Non-SE polygon has a low number of (or no) disperse sensed voxels. An SE polygon additionally contains *sensed* and *non-sensed structural voxels* (see Fig. 58.3a for a better understanding of this).

In this labelled voxel space, a sorted list of next best scanner positions $\{l\}_{NBTS}$ is determined by means of a certainty function. This is formulated in probabilistic terms by means of the SE membership probability which, for a voxel, is defined as the probability of it being labelled as a *sensed structural voxel* in the next scan.

As is explained below in more detail, the robot then calculates an obstacle map (OM) and selects the next best scan position from among the former list of candidates. The first free path, according to the global path planning algorithm, is chosen. Finally, the robot moves using its own local planner and reaches its final position. Figure 58.3b shows the thermal models calculated after the first and third scans.

58.4.2 Robot Navigation and Integrated 3D Thermal Model

Assuming that the list of the next best positions $\{l\}_{NBTS}$ has been calculated, we distinguish three principal stages in the robot navigation: the current obstacle map, the best path and the movement of the robot.

The current obstacle map is an image that the robot uses for a safe navigation. The first version is built by performing a top-projection of the horizontal data slice which goes from the ground to the height of the MoPATD. Data above the MoPATD obviously have no influence on the navigation of the robot. On this obstacle map, it is assumed that a black pixel signifies an obstacle and a white pixel represents a free position. Owing to the size of the MoPATD and the security requirements (the robot must be a certain distance from the obstacles), the free space in the first OM version is highly

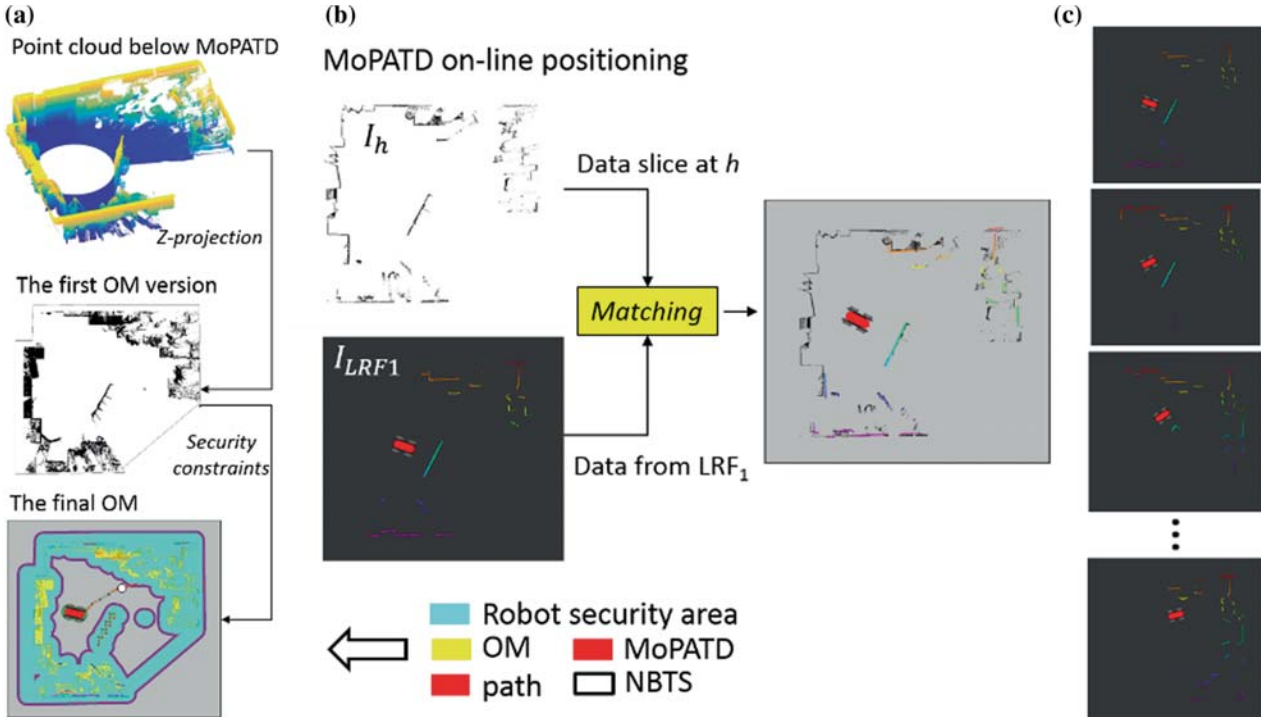

Fig. 58.4 **a** Localizing MoPATD in OM. A view of the data below the height of the MoPATD (left), the initial OM (centre) and the final OM (right). The security regions are shown in cyan and the free positions are in grey. The next best position of the robot and the path calculated by the Navfn planner are included. **b** MoPATD navigation. Result obtained after matching I_h and I_{LRF1} (above). **c** A sequence of images I_{LRF1} from the origin to the end point

reduced to a second version, in which the robot can safely navigate. Taking all this into account, the first candidate in the list $\{I\}_{NBTS}$ that lies in a free region is chosen as the definitive next best position of the scanner (see Fig. 58.4a).

The path from the current to the next position is obtained using the Navfn planner, which runs under ROS (Robot Operating System). This planner uses a costmap to find the minimum cost path from the start point to the end point in a gridded OM. The navigation function is computed using the Dijkstra algorithm.

When the MoPATD moves, a robot positioning algorithm must be run. This signifies that the robot must know, at any moment, its precise position inside the OM. In order to match the information provided by the frontal laser range finder (i.e. LRF1) with the calculated OM, we place LRF1 near the base of the laser scanner, at a certain height h. The information read by LRF1, denominated as I_{LRF1}, can thus be matched to a narrow slice of points at this vertical height h. The map generated by this data slice, which we denote as I_h, is taken as a positioning reference (see illustration in Fig. 58.4b). The robot localizes itself by means of the Adaptive Monte Carlo Localization (AMCL) algorithm.

A new 360-thermal scan must be registered in the world coordinate system, which was established by the first position of the scanner. In order to ensure an efficient registration of a new scan, the odometry of the robot first provides an approximate transformation between the last and the current robot positions. This coarse registration is later refined by using the ICP algorithm.

The scanning process is repeated until a particular stopping criterion is satisfied. The stopping criterion is based on two threshold parameters: the percentage of the SE areas that has been sensed (according to the current RoI) and the increase in the sensed SE area with respect to the last thermal scan. These parameters were set empirically at 90 and 1%, respectively. At the end of this process, the thermal point cloud of the architectural structure of the indoor of the building is generated.

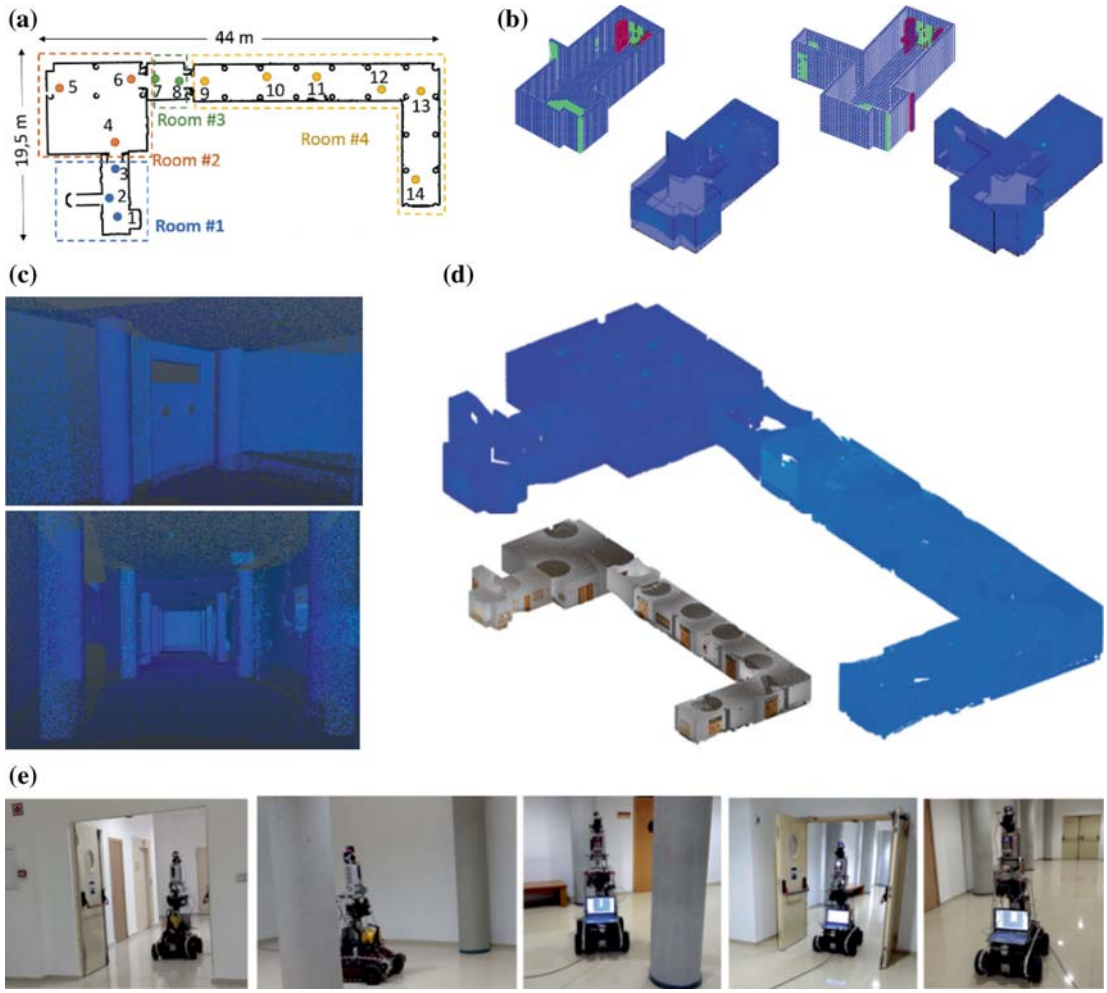

Fig. 58.5 **a** Blueprint of the scene with positions of MoPATD during the scanning session. **b** Evolution of the voxel space and the thermal model in room #1. **c** Some views of the thermal model of the scene. **d** The 3D thermal model. **e** Photos of MoPATD

58.5 Experimental Test

In this section, we present the results obtained for MoPATD on a representative case study. The scene consisted of several rooms in the basement of the Industrial Engineering School at Castilla-La Mancha University, Spain.

The scene is 858 m^2 in size with four lecture halls that are 3.15 m high. The scenario has a large number of columns (24), different kinds of doors (31) and SEs (40). Rooms #2 and #4 are particularly large. MoPATD started scanning this scenario in room #1 and entered the remaining rooms by following the order shown in Fig. 58.5a. In total, the platform stopped in 14 positions and collected 51 million thermal data.

As mentioned in Sect. 58.2, the robot moves until the stopping criteria are verified. At this point of the process, the system runs the door detection algorithm and the platform goes towards the open door that leads to the next room. The robot then stops one meter in front of the door, takes the last scan of the room, passes through the door and stops one meter away from the door. The first scan of the new room is then taken and the process starts again. This is the most critical problem in the whole experiment. Fortunately, the system detected the doors and successfully entered the new room in 100% of the cases. In addition, there was a 95% of successfully identified SEs and a 5% of false negatives.

An example of the evolution of the voxel space and the thermal models calculated in room #1 is illustrated in Fig. 58.5b. Figure 58.5c, d represent some views of the thermal model in rooms and the total thermal model and Fig. 58.5e shows some photos of MoPATD moving in the scenario and passing through doors.

Some interesting time data as regards different steps of the scanning process follows. The scanning session took a total of 1.29 h. The system spent most of the time collecting (43%) and transferring (21.3%) data. The time percentages for the rest of the processes were: identification of outliers (5%), registration (1.3%), RoI (5%), NBTS (15.3%) and the movement of the robot (9.2%).

58.6 Conclusions

This paper presents MoPATD, an autonomous platform that provides a 3D thermal model of the architectural structure of the indoors of a building. The system is able to decide the next best scan position based on the current information of the structure of the building, and navigates from one position to another until a room is completely sensed. MoPATD subsequently moves towards the door of the room, enters the adjoining room and begins the scanning process. This system is one of the few platforms in the world with this degree of autonomy. MoPATD has been successfully tested in real environments.

However, the current version of MoPATD has evident limitations that need to be tackled and some improvements will hopefully be made in the next few months. One of the current problems is that the system takes and processes very-high density point clouds (above one data/cm^2) which, for very large rooms, entails excessive memory and time resources. This high data density is required for the precise detection of doors and, especially, small building components on walls (e.g. sockets, switches and signs), (see [12]). However, thermal maps do not require this degree of resolution and could be constructed faster and with much fewer memory requirements. Another important aspect is that MoPATD moves to an adjoining room only when the door is open. We aim to develop a manipulator robot that will be coupled to MoPATD, and that will be able to open closed doors.

Acknowledgements This work has been supported by the Spanish Ministry of Economy and Competitiveness [DPI2016-76380-R project] and by the University of Castilla-La Mancha [PREDUCLM16/23 human resources grant].

References

1. Cho, Y.K., Ham, Y., Golpavar-Fard, M.: 3D as-is building energy modeling and diagnostics: a review of the state-of-the-art. Adv. Eng. Inf. **29**, 184–195 (2015). https://doi.org/10.1016/j.aei.2015.03.004
2. Wang, C., Cho, Y.K., Gai, M.: As-is 3D thermal modeling for existing building envelopes using a hybrid LIDAR system. J. Comput. Civ. Eng. **27**, 645–656 (2013). https://doi.org/10.1061/(ASCE)CP.1943-5487.0000273
3. Ham, Y., Golparvar-Fard, M.: An automated vision-based method for rapid 3D energy performance modeling of existing buildings using thermal and digital imagery. Adv. Eng. Inf. **27**, 395–409 (2013). https://doi.org/10.1016/j.aei.2013.03.005
4. Rangel, J., Soldan, S., Kroll, A., Rangel, J., Kroll, A., Soldan, S., Kroll, A.: 3D Thermal imaging: fusion of thermography and depth cameras. In: International Conference on Quantitative Infra Red Thermography (2014)
5. Armesto, J., Sánchez-Villanueva, C., Patiño-Cambeiro, F., Patiño-Barbeito, F.: Indoor multi-sensor acquisition system for projects on energy renovation of buildings. Sensors (Switzerland) **16**, 1–14 (2016). https://doi.org/10.3390/s16060785
6. Mader, D., Blaskow, R., Westfeld, P., Weller, C.: Potential of UAV-Based laser scanner and multispectral camera data in building inspection. ISPRS Int. Arch. Photogram. Remote Sens. Spat. Inf. Sci. **XLI-B1**, 1135–1142 (2016). https://doi.org/10.5194/isprsarchives-xli-b1-1135-2016
7. Borrmann, D., Nüchter, A., Đakulović, M., Maurović, I., Petrović, I., Osmanković, D., Velagić, J., Maurovic, I., Petrović, I., Osmankovic, D., Velagić, J.: A mobile robot based system for fully automated thermal 3D mapping. Adv. Eng. Inf. **28**, 425–440 (2014). https://doi.org/10.1016/j.aei.2014.06.002
8. Heikkila, J., Silven, O.: A four-step camera calibration procedure with implicit image correction. In: IEEE Computer Society Conference on Computer Vision and Pattern Recognition, pp. 1106–1112 (1997)
9. Blaer, P.S., Allen, P.K.: Data acquisition and view planning for 3-D modeling tasks. In: IEEE IROS, pp. 417–422, San Diego, CA (2007)
10. Potthast, C., Sukhatme, G.S.: A probabilistic framework for next best view estimation in a cluttered environment. J. Vis. Commun. Image Represent. **25**, 148–164 (2014). https://doi.org/10.1016/j.jvcir.2013.07.006
11. Quintana, B., Prieto, S.A., Adán, A., Vázquez, A.S.: Semantic scan planning for indoor structural elements of buildings. Adv. Eng. Inf. **30**, 643–659 (2016). https://doi.org/10.1016/j.aei.2016.08.003
12. Adán, A., Quintana, B., Prieto, S.A., Bosché, F.: Scan-to-BIM for "secondary" building components. Adv. Eng. Inf. **37**, 119–138 (2018)